Int J Theor Phys (2008) 47: 772–796
DOI 10.1007/s10773-007-9502-3

Transverse Wave Propagation in Relativistic Two-Fluid Plasmas around Reissner–Nordström Black Hole

M. Hossain Ali · M. Atiqur Rahman

Received: 19 May 2007 / Accepted: 20 July 2007 / Published online: 29 August 2007
© Springer Science+Business Media, LLC 2007

Abstract We investigate transverse electromagnetic waves propagating in a plasma influenced by the gravitational field of the Reissner–Nordström black hole. Applying $3+1$ spacetime split we reformulate the relativistic two-fluid equations to take account of gravitational effects due to the event horizon and describe the set of simultaneous linear equations for the perturbations. Using a local approximation we investigate the one-dimensional radial propagation of Alfvén and high frequency electromagnetic waves. We derive the dispersion relation for these waves and solve it for the wave number k numerically.

Keywords Two fluid plasma · Alfvén and high frequency electromagnetic waves · Event horizon · Charged black hole

1 Introduction

In recent years there has been a renewed interest in investigating plasmas in the black hole environment. A successful study of the waves and emissions from plasmas falling into a black hole will be of great value in aiding the observational identification of black hole candidates.

A covariant formulation of the theory based on the fluid equations in curved spacetime has so far proved unproductive because of the curvature of four-dimensional spacetime in the region surrounding a black hole.

Thorne, Price, and Macdonald (TPM) [1–4] developed a method of a $3+1$ formulation of general relativity in which the electromagnetic equations and the plasma physics at least look somewhat similar to the usual formulations in flat spacetime while taking accurate account of general relativistic effects such as curvature. In the TPM formulation, work connected with black holes has been facilitated by replacing the hole's event horizon with a

M. Hossain Ali (✉) · M. Atiqur Rahman
Department of Applied Mathematics, Rajshahi University, Rajshahi 6205, Bangladesh
e-mail: m_hossain_ali_bd@yahoo.com

M. Atiqur Rahman
e-mail: atirubd@yahoo.com

membrane endowed with electric charge, electrical conductivity, and finite temperature and entropy. The membrane paradigm is mathematically equivalent to the standard, full general relativistic theory of black holes so far as physics outside the event horizon is concerned. But the formulation of all physics in this region turns out to be very much simpler than it would be using the standard covariant approach of general relativity.

Zheng [5, 6] exploited this approach, considering ideal magnetohydrodynamics (MHD) waves near the Kerr black hole, to account for the effects of the hole's angular momentum, ignoring the effects due to the black hole horizon. Some other authors [7–9] used the $3+1$ formulation to investigate some properties of wave propagation in the Friedmann universe.

Actually the $3+1$ approach was originally developed in 1962 by Arnowitt, Deser, and Misner [10] to study the quantization of the gravitational field. Since then, their formulation has most been applied in studying numerical relativity [11]. TPM extended the $3+1$ formalism to include electromagnetism and applied it to study electromagnetic effects near the Kerr black hole.

Recently, Buzzi, Hines, and Treumann (BHT) [12, 13], using the $3+1$ formalism, described a general relativistic version of two-fluid formulation of plasma physics, developed a linearized treatment of plasma waves in analogy with the special relativistic formulation of Sakai and Kawata (SK) [14], and applied it to investigate the nature of the waves (transverse waves in [12], longitudinal waves in [13]) near the horizon of the Schwarzschild black hole.

In this paper we apply linearized two-fluid equations of BHT to investigate transverse electromagnetic waves propagating in a plasma close to the Reissner–Nordström (RN) black hole, which is the Schwarzschild black hole generalized with the charge parameters: electric as well as magnetic monopole charges. The magnetic monopole hypothesis was propounded by Dirac relatively long ago. The ingenious suggestion by Dirac that magnetic monopole does exist was neglected due to the failure to detect such a particle. However, in recent years the development of gauge theories has shed new light on it. In extreme case the RN black hole is distinguished by its coldness (vanishing Hawking temperature) and its supersymmetry. It occupies a special position among the solutions to Einstein or Einstein–Maxwell equations because of its complete stability with respect to both classical and quantum process permitting its interpretation as a soliton [15, 16]. The extremal RN space is also special in admitting supersymmetry in the contest of $N=2$ supergravity [16–21]. Thus aspects of the RN solution must be of interest in a broader contest. In view of these reasons, our study of transverse wave propagation in relativistic two-fluid plasma in the environment close to the event horizon of the RN black hole is interesting. The result we obtained reduces to that of the Schwarzschild black hole [12] when the charge term vanishes.

This paper is organized as follows. In Sect. 2 we summarize the $3+1$ formulation of general relativity. In Sect. 3 we describe the nonlinear two-fluid equations expressing continuity and conservation of energy and momentum. The two-fluids are coupled together through Maxwell's equations for the electromagnetic fields. For zero gravitational fields these equations reduce to the corresponding special relativistic expressions. In Sect. 4 we restrict one-dimensional wave propagation in the radial z (Rindler coordinate system) direction, and linearize the equations for wave propagation in Sect. 5 by giving a small perturbation to fields and fluid parameters. We express the derivatives of the unperturbed quantities with respect to z. In Sect. 6 we discuss the local, or mean-field, approximation used to obtain numerical solutions for the wave dispersion relations. We describe the dispersion relation for the transverse waves in Sect. 7, and give the numerical procedure for determining the roots of the dispersion relation in Sect. 8. In Sect. 9 we present the numerical solutions for the wave number k. Finally, in Sect. 10 we present our remarks. We use units $G=c=k_B=1$.

2 3 + 1 Spacetime Formalism

The $3+1$ formulation of general relativity developed by TPM [1–4] is based on the concept of selecting a preferred set of spacelike hypersurfaces which form the level surfaces of a congruence of timelike curves. A particular set of these hypersurfaces constitutes a time slicing of spacetime. The hypersurfaces considered here are of constant universal time t. In this section we apply TPM formulation to split the Reissner–Nordström spacetime which has the metric

$$ds^2 = g_{\mu\nu}dx^\mu dx^\nu = -\Delta^2 dt^2 + \frac{1}{\Delta^2}dr^2 + r^2(d\theta^2 + \sin^2\theta d\varphi^2),$$
$$\Delta^2 = 1 - \frac{2M}{r} + \frac{q^2}{r^2}, \quad q^2 = q_e^2 + q_m^2 \tag{1}$$

together with a vector potential with nonvanishing components: $A_t = q_e/r$, $A_\varphi = -q_m\cos\theta$. Here, M is the mass, q_e the electric charge, and q_m the magnetic charge of the black hole. The components x^μ denote spacetime coordinates and $\mu,\ \nu = 0, 1, 2, 3$. The spacetime (1) has a curvature singularity at $r = 0$ as for Schwarzschild, but in addition has two horizons where g_{tt} vanishes:

$$r_\pm = M \pm \sqrt{M^2 - q^2}. \tag{2}$$

There is an event horizon at $r = r_+$ and an inner (Cauchy) horizon at $r = r_-$. For $q < M$ the singularity at $r = 0$ is hidden behind these horizons, while for $q > M$ there exists no real root of (2) and the spacetime has a naked singularity.

The case $M = q$ gives the extremal RN black hole spacetime, which has special properties. At the classical level, this spacetime is just on the verge of developing a naked singularity. For $q = 0$, the extremal spacetime is just the flat space vacuum. Even for non-zero q, the extremal spacetime can be thought of as the vacuum in the charge q sector of the theory [22]. The extremal spacetime is also singled out in the context of supergravity, in that it is the solution of the supergravity equations of motion which preserve half of the supersymmetries [23].

A charged black hole preferentially radiates away its charge, the amount of which depends on the charge to mass ratio. If this ratio is sufficiently small, most of the radiation is in the form of neutral particles and q is essentially constant. This is likely to be true for magnetically charged black holes. In this case, the black hole evolves toward its extremal limit. The Hawking temperature [24]

$$T_H = \frac{\sqrt{M^2 - q^2}}{2\pi(M + \sqrt{M^2 - q^2})}$$

vanishes as $q \to M$, and hence, extremal charged black holes may be quantum mechanically stable. There is a possibility that extremal quantum black holes can bifurcate [25], but this is consistent with ideas of cosmic censorship. As the black hole approaches the extremal limit, the Hawking radiation turns off. It does not continue to radiate to a naked singularity.

An absolute three-dimensional space defined by the hypersurfaces of constant universal time t is described by the metric

$$ds^2 = g_{ij}dx^i dx^j = \frac{1}{\Delta^2}dr^2 + r^2(d\theta^2 + \sin^2\theta d\varphi^2). \tag{3}$$

The indices i, j range over $1, 2, 3$ and refer to coordinates in absolute space. The fiducial observers (FIDOs), i.e. the observers remaining at rest with respect to this absolute space, measure their proper time τ using clocks that they carry with them and make local measurements of physical quantities. Then all their measured quantities are defined as FIDO locally measured quantities and all rates measured by them are measured using FIDO proper time. The FIDOs use a local Cartesian coordinate system with unit basis vectors tangent to the coordinate lines

$$\mathbf{e}_{\hat{r}} = \Delta \frac{\partial}{\partial r}, \qquad \mathbf{e}_{\hat{\theta}} = \frac{1}{r}\frac{\partial}{\partial \theta}, \qquad \mathbf{e}_{\hat{\varphi}} = \frac{1}{r\sin\theta}\frac{\partial}{\partial \varphi}. \tag{4}$$

For a spacetime viewpoint rather than a $3+1$ split of spacetime, the set of orthonormal vectors also includes the basis vector for the time coordinate given by

$$\mathbf{e}_{\hat{0}} = \frac{d}{d\tau} = \frac{1}{\alpha}\frac{\partial}{\partial t}, \tag{5}$$

where α is the lapse function (or redshift factor) defined by

$$\alpha(r) \equiv \frac{d\tau}{dt} = \frac{1}{r}(r - r_+)^{\frac{1}{2}}(r - r_-)^{\frac{1}{2}}. \tag{6}$$

The gravitational acceleration felt by a FIDO is given by [1–4]

$$\mathbf{a} = -\nabla \ln\alpha = -\frac{1}{\alpha}\left(\frac{M}{r^2} - \frac{q^2}{r^3}\right)\mathbf{e}_{\hat{r}}, \tag{7}$$

while the rate of change of any scalar physical quantity or any three-dimensional vector or tensor, as measured by a FIDO, is defined by the convective derivative

$$\frac{D}{D\tau} \equiv \left(\frac{1}{\alpha}\frac{\partial}{\partial t} + \mathbf{v}\cdot\nabla\right), \tag{8}$$

$\mathbf{v}$ being the velocity of a fluid as measured locally by a FIDO.

3 Two Fluid Equations in 3 + 1 Formalism

In this section we describe the equations for continuity, the conservation of energy and momentum, and Maxwell's equations in $3+1$ formalism. We consider two-component plasma such as electron-positron plasma or electron-ion plasma. In the $3+1$ notation, the continuity equation for each of the fluid species is

$$\frac{\partial}{\partial t}(\gamma_s n_s) + \nabla\cdot(\alpha\gamma_s n_s \mathbf{v}_s) = 0, \tag{9}$$

where s is 1 for electrons and 2 for positrons (or ions). For a perfect relativistic fluid of species s in three-dimensions, the energy density ϵ_s, the momentum density $\mathbf{S}_s$, and stress-energy tensor W_s^{jk} are given by

$$\epsilon_s = \gamma_s^2(\varepsilon_s + P_s\mathbf{v}_s^2), \qquad \mathbf{S}_s = \gamma_s^2(\varepsilon_s + P_s)\mathbf{v}_s, \qquad W_s^{ik} = \gamma_s^2(\varepsilon_s + P_s)v_s^j v_s^k + P_s g^{jk}, \tag{10}$$

where $\mathbf{v}_s$ is the fluid velocity, n_s is the number density, P_s is the pressure, and ε_s is the total energy density defined by

$$\varepsilon_s = m_s n_s + P_s/(\gamma_g - 1), \tag{11}$$

where the gas constant γ_g is $4/3$ for $T \to \infty$ and $5/3$ for $T \to 0$.

The ion temperature profile is closely adiabatic and it approaches 10^{12} K near the horizon [26]. Far from the (event) horizon electron (positron) temperatures are essentially equal to the ion temperatures, but closer to the horizon the electrons are progressively cooled to about 10^8–10^9 K by mechanisms like multiple Compton scattering and synchrotron radiation.

Using the conservation of entropy, the equation of state can be expressed by

$$\frac{D}{D\tau}\left(\frac{P_s}{n_s^{\gamma_g}}\right), \tag{12}$$

where $D/D\tau = (1/\alpha)\partial/\partial t + \mathbf{v}_s \cdot \nabla$. The full equation of state for a relativistic fluid, as measured in the fluid's rest frame, is as follows [27, 28]:

$$\varepsilon_s = m_s n_s + m_s n_s \left[\frac{P_s}{m_s n_s} - \frac{\mathrm{i}H_2^{(1)'}(\mathrm{i}m_s n_s/P_s)}{\mathrm{i}H_2^{(1)}(\mathrm{i}m_s n_s/P_s)}\right], \tag{13}$$

where the $H_2^{(1)}(x)$ are Hankel functions.

The quantities of (10) in the electromagnetic field are expressed in the following form:

$$\begin{aligned} \epsilon_s &= \frac{1}{8\pi}(\mathbf{E}^2 + \mathbf{B}^2), \qquad \mathbf{S}_s = \frac{1}{4\pi}\mathbf{E} \times \mathbf{B}, \\ W_s^{jk} &= \frac{1}{8\pi}(\mathbf{E}^2 + \mathbf{B}^2)g^{jk} - \frac{1}{4\pi}(E^j E^k + B^j B^k). \end{aligned} \tag{14}$$

The conservation of energy and momentum equations are written, respectively, as follows [1–3]:

$$\frac{1}{\alpha}\frac{\partial}{\partial t}\epsilon_s = -\nabla \cdot \mathbf{S}_s + 2\mathbf{a} \cdot \mathbf{S}_s, \tag{15}$$

$$\frac{1}{\alpha}\frac{\partial}{\partial t}\mathbf{S}_s = \epsilon_s \mathbf{a} - \frac{1}{\alpha}\nabla \cdot (\alpha \overleftrightarrow{\mathbf{W}}_s). \tag{16}$$

When the two-fluid plasma couples to the electromagnetic fields, Maxwell's equations take the following form:

$$\nabla \cdot \mathbf{B} = 0, \tag{17}$$

$$\nabla \cdot \mathbf{E} = 4\pi\sigma, \tag{18}$$

$$\frac{\partial \mathbf{B}}{\partial t} = -\nabla \times (\alpha \mathbf{E}), \tag{19}$$

$$\frac{\partial \mathbf{E}}{\partial t} = \nabla \times (\alpha \mathbf{B}) - 4\pi\alpha \mathbf{J}, \tag{20}$$

where the charge and current densities are defined by

$$\sigma = \sum_s \gamma_s q_s n_s, \qquad \mathbf{J} = \sum_s \gamma_s q_s n_s \mathbf{v}_s. \tag{21}$$

Using (11) and (17–20), the energy and momentum conservation equations (15) and (16) can be rewritten for each species s in the form

$$\frac{1}{\alpha}\frac{\partial}{\partial t}P_s - \frac{1}{\alpha}\frac{\partial}{\partial t}[\gamma_s^2(\varepsilon_s + P_s)] - \nabla\cdot[\gamma_s^2(\varepsilon_s + P_s)\mathbf{v}_s] + \gamma_s q_s n_s \mathbf{E}\cdot\mathbf{v}_s + 2\gamma_s^2(\varepsilon_s + P_s)\mathbf{a}\cdot\mathbf{v}_s = 0, \tag{22}$$

$$\gamma_s^2(\varepsilon_s + P_s)\left(\frac{1}{\alpha}\frac{\partial}{\partial t} + \mathbf{v}_s\cdot\nabla\right)\mathbf{v}_s + \nabla P_s - \gamma_s q_s n_s(\mathbf{E} + \mathbf{v}_s\times\mathbf{B}) + \mathbf{v}_s\left(\gamma_s q_s n_s \mathbf{E}\cdot\mathbf{v}_s + \frac{1}{\alpha}\frac{\partial}{\partial t}P_s\right) + \gamma_s^2(\varepsilon_s + P_s)[\mathbf{v}_s(\mathbf{v}_s\cdot\mathbf{a}) - \mathbf{a}] = 0. \tag{23}$$

Although these equations are valid in a FIDO frame, they reduce for $\alpha = 1$ to the corresponding special relativistic equations as given by SK [14] which are valid in a frame in which both fluids are at rest. The transformation from the FIDO frame to the comoving (fluid) frame involves a boost velocity, which is simply the freefall velocity onto the black hole, given by

$$v_{\rm ff} = (1-\alpha^2)^{\frac{1}{2}}. \tag{24}$$

Then the relativistic Lorentz factor $\gamma_{\rm boost} \equiv (1 - v_{\rm ff}^2)^{-1/2} = 1/\alpha$.

The Rindler coordinate system, in which space is locally Cartesian, provides a good approximation to the Reissner–Nordström metric near the event horizon in the form

$$ds^2 = -\Delta^2 dt^2 + dx^2 + dy^2 + dz^2, \tag{25}$$

where

$$x = r_+\left(\theta - \frac{\pi}{2}\right), \qquad y = r_+\varphi, \qquad z = 2r_+\Delta^2. \tag{26}$$

The standard lapse function in Rindler coordinates becomes $\alpha = z/2r_+$, where r_+ is the event horizon of the black hole.

4 One-Dimensional Radial Wave Propagation

We consider one-dimensional wave propagation in the radial z direction and introduce the complex variables

$$\begin{aligned} &v_{sz}(z,t) = u_s(z,t), \qquad v_s(z,t) = v_{sx}(z,t) + \mathrm{i}v_{sy}(z,t),\\ &B(z,t) = B_x(z,t) + \mathrm{i}B_y(z,t), \qquad E(z,t) = E_x(z,t) + \mathrm{i}E_y(z,t). \end{aligned} \tag{27}$$

Then

$$\begin{aligned} v_{sx}B_y - v_{sy}B_x &= \frac{\mathrm{i}}{2}(v_s B^* - v_s^* B),\\ v_{sx}E_y - v_{sy}E_x &= \frac{\mathrm{i}}{2}(v_s E^* - v_s^* E), \end{aligned} \tag{28}$$

where the $*$ denotes the complex conjugate. The continuity equation (9) takes the form

$$\frac{\partial}{\partial t}(\gamma_s n_s) + \frac{\partial}{\partial z}(\alpha\gamma_s n_s u_s) = 0, \tag{29}$$

while Poisson's equation (18) becomes

$$\frac{\partial E_z}{\partial z} = 4\pi(q_1 n_1 \gamma_1 + q_2 n_2 \gamma_2). \tag{30}$$

The $\mathbf{e}_{\hat{x}}$ and $\mathbf{e}_{\hat{y}}$ components of (19) and (20) give

$$\frac{1}{\alpha}\frac{\partial B}{\partial t} = -\mathrm{i}\left(\frac{\partial}{\partial z} - a\right)E, \tag{31}$$

$$\mathrm{i}\frac{\partial E}{\partial t} = -\alpha\left(\frac{\partial}{\partial z} - a\right)B - \mathrm{i}4\pi e\alpha(\gamma_2 n_2 v_2 - \gamma_1 n_1 v_1). \tag{32}$$

Differentiating (32) with respect to t and using (31), we obtain

$$\left(\alpha^2\frac{\partial^2}{\partial z^2} + \frac{3\alpha}{2r_+}\frac{\partial}{\partial z} - \frac{\partial^2}{\partial t^2} + \frac{1}{(2r_+)^2}\right)E = 4\pi e\alpha\frac{\partial}{\partial t}(n_2\gamma_2 v_2 - n_1\gamma_1 v_1). \tag{33}$$

From the $\mathbf{e}_{\hat{x}}$ and $\mathbf{e}_{\hat{y}}$ components of (23) the transverse component of the momentum conservation equation is

$$\rho_s\frac{Dv_s}{D\tau} = q_s n_s\gamma_s(E - \mathrm{i}v_s B_z + \mathrm{i}u_s B) - u_s v_s\rho_s a - v_s\left(q_s n_s\gamma_s\mathbf{E}\cdot\mathbf{v}_s + \frac{1}{\alpha}\frac{\partial P_s}{\partial t}\right), \tag{34}$$

where

$$\mathbf{E}\cdot\mathbf{v}_s = \frac{1}{2}(Ev_s^* + E^* v_s) + E_z u_s$$

and ρ_s is the total energy density defined by

$$\rho_s = \gamma_s^2(\varepsilon_s + P_s) = \gamma_s^2(m_s n_s + \Gamma_g P_s) \tag{35}$$

with $\Gamma_g = \gamma_g/(\gamma_g - 1)$.

5 Linearization

We linearize the equations derived in the preceding section by perturbation method. We introduce the quantities

$$\begin{aligned}
u_s(z,t) &= u_{0s}(z) + \delta u_s(z,t), & v_s(z,t) &= \delta v_s(z,t),\\
n_s(z,t) &= n_{0s}(z) + \delta n_s(z,t), & P_s(z,t) &= P_{0s}(z) + \delta P_s(z,t),\\
\rho_s(z,t) &= \rho_{0s}(z) + \delta\rho_s(z,t), & \mathbf{E}(z,t) &= \delta\mathbf{E}(z,t),\\
\mathbf{B}_z(z,t) &= \mathbf{B}_0(z) + \delta\mathbf{B}_z(z,t), & \mathbf{B}(z,t) &= \delta\mathbf{B}(z,t).
\end{aligned} \tag{36}$$

Here, magnetic field has been chosen to lie along the radial $\mathbf{e}_{\hat{z}}$ direction. The relativistic Lorentz factor is also linearized such that

$$\gamma_s = \gamma_{0s} + \delta\gamma_s, \quad \text{where } \gamma_{0s} = \left(1 - \mathbf{u}_{0s}^2\right)^{-\frac{1}{2}},\ \delta\gamma_s = \gamma_{0s}^3\mathbf{u}_{0s}\cdot\delta\mathbf{u}_s. \tag{37}$$

The unperturbed radial velocity near the event horizon for each species as measured by a FIDO along $\mathbf{e}_{\hat{z}}$ is assumed to be the freefall velocity so that

$$u_{0s}(z) = v_{\mathrm{ff}}(z) = [1 - \alpha^2(z)]^{\frac{1}{2}}. \tag{38}$$

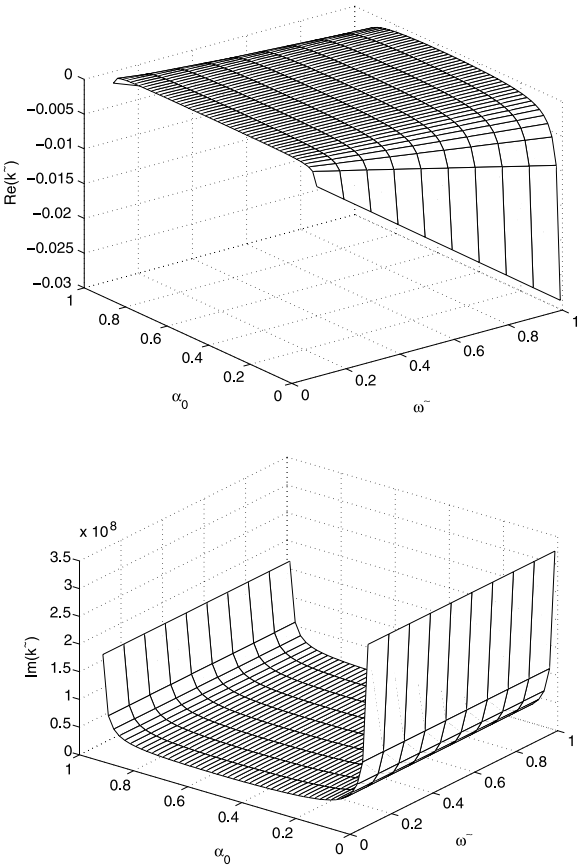

Fig. 1 *Top*: Real part of Alfvén mode for the electron-positron plasma. *Bottom*: Imaginary part of Alfvén damped mode

From the continuity equation (29), it follows that

$$r^2\alpha\gamma_{0s}n_{0s}u_{0s} = \text{const.} = r_+^2\alpha_+\gamma_+n_+u_+,$$

where the values with a subscript + are the limiting values at the event horizon. The freefall velocity at the horizon becomes unity so that $u_+ = 1$. Since $u_{0s} = v_{\text{ff}}$, $\gamma_{0s} = 1/\alpha$; and hence $\alpha\gamma_{0s} = \alpha_+\gamma_+ = 1$. Also, because $v_{\text{ff}} = \zeta(r_+/r)^{1/2}$, the number density for each species can be written as follows:

$$n_{0s}(z) = \frac{1}{\zeta^4}n_{+s}v_{\text{ff}}^3(z), \tag{39}$$

where

$$\zeta = \left[1 + \frac{r_-}{r_+}\left(1 - \frac{r_+}{r}\right)\right]^{\frac{1}{2}}. \tag{40}$$

The equation of state (12) and (40) lead to write the unperturbed pressure, in terms of the freefall velocity, as follows:

$$P_{0s}(z) = P_{+s}v_{\text{ff}}^{3\gamma_g}(z). \tag{41}$$

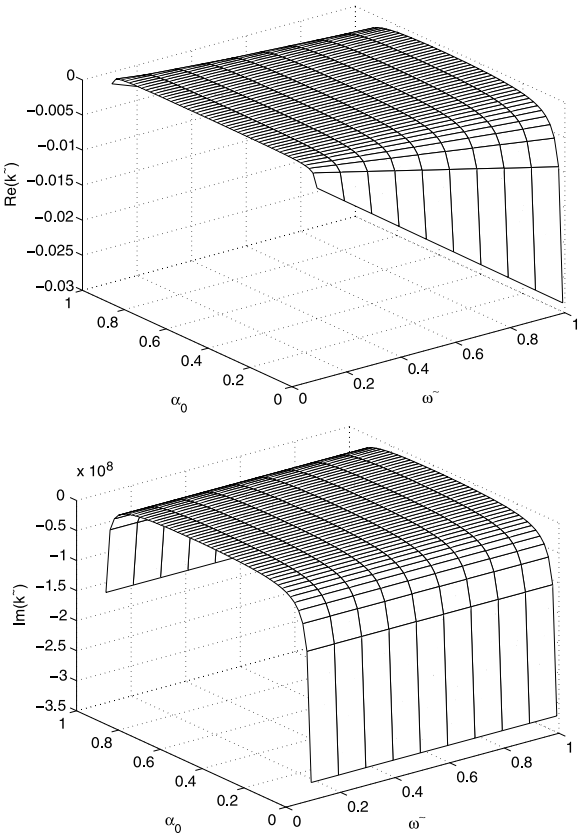

Fig. 2 *Top*: Real part of Alfvén mode for the electron-positron plasma. *Bottom*: Imaginary part of Alfvén growth mode

Since $P_{0s} = k_B n_{0s} T_{0s}$, then with $k_B = 1$, the temperature profile is

$$T_{0s} = T_{+s} v_{\rm ff}^{3(\gamma_g - 1)}(z). \tag{42}$$

The unperturbed magnetic field is purely in the radial direction. It does not experience effects of spatial curvature. From the flux conservation $\nabla \cdot \mathbf{B}_0 = 0$ it follows that

$$r^2 B_0(r) = \text{const.}$$

from which one obtains the unperturbed magnetic field, in terms of the freefall velocity, in the form

$$B_0(z) = B_+ v_{\rm ff}^4(z), \tag{43}$$

where $v_{\rm ff} = [1 - \alpha^2(z)]^{1/2}$. Since

$$\frac{dv_{\rm ff}}{dz} = -\frac{\alpha}{2r_+}\frac{1}{v_{\rm ff}}, \tag{44}$$

we have

$$\frac{du_{0s}}{dz} = -\frac{\alpha}{2r_+}\frac{1}{v_{\rm ff}}, \qquad \frac{dB_0}{dz} = -\frac{4\alpha}{2r_+}\frac{B_0}{v_{\rm ff}^2},$$

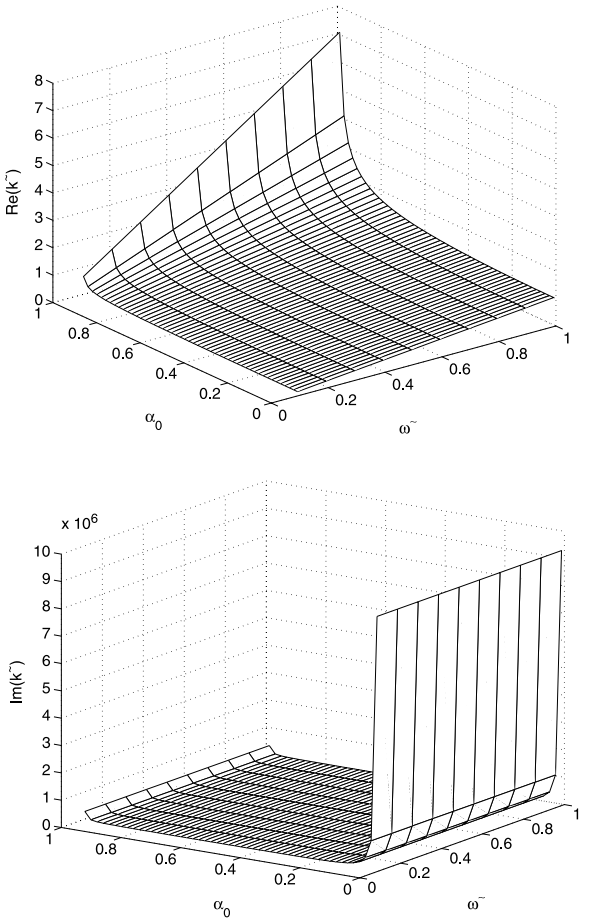

Fig. 3 *Top*: Real part of Alfvén mode for the electron-positron plasma. *Bottom*: Imaginary part of Alfvén damped mode

$$\frac{dn_{0s}}{dz} = -\frac{3\alpha}{2r_+}\frac{n_{0s}}{v_{\mathrm{ff}}^2}, \qquad \frac{dP_{0s}}{dz} = -\frac{3\alpha}{2r_+}\frac{\gamma_g P_{0s}}{v_{\mathrm{ff}}^2}. \tag{45}$$

When the linearized variables from (36) and (37) are substituted into the continuity equation and products of perturbation terms are neglected, it follows that

$$\gamma_{0s}\left(\frac{\partial}{\partial t} + u_{0s}\alpha\frac{\partial}{\partial z} + \frac{u_{0s}}{2r_+} + \gamma_{0s}^2\alpha\frac{du_{0s}}{dz}\right)\delta n_s + \left(\alpha\frac{\partial}{\partial z} + \frac{1}{2r_+}\right)(n_{0s}\gamma_{0s}u_{0s}) + n_{0s}\gamma_{0s}^3\left[u_{0s}\frac{\partial}{\partial t} + \alpha\frac{\partial}{\partial z} + \frac{1}{2r_+} + \alpha\left(\frac{1}{n_{0s}}\frac{dn_{0s}}{dz} + 3\gamma_{0s}^2u_{0s}\frac{du_{0s}}{dz}\right)\right]\delta u_s = 0. \tag{46}$$

Doing the same we obtain from the conservation of entropy, (12),

$$\delta P_s = \frac{\gamma_g P_{0s}}{n_{0s}}\delta n_s, \tag{47}$$

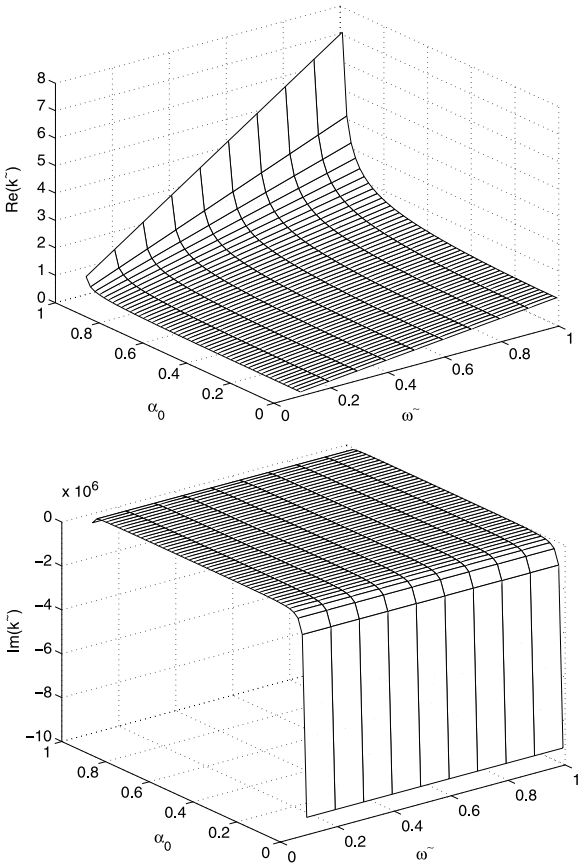

Fig. 4 *Top*: Real part of Alfvén mode for the electron-positron plasma. *Bottom*: Imaginary part of Alfvén growth mode

and from the total energy density, (35),

$$\delta\rho_s = \frac{\rho_{0s}}{n_{0s}}\left(1 + \frac{\gamma_{0s}^2\gamma_g P_{0s}}{\rho_{0s}}\right)\delta n_s + 2u_{0s}\gamma_{0s}^2\rho_{0s}\delta u_s, \tag{48}$$

where $\rho_{0s} = \gamma_{0s}^2(m_s n_{0s} + \Gamma_g P_{0s})$. When the transverse part of the momentum conservation equation is linearized, differentiated with respect to t, and substituted from (31), it gives

$$\left(\alpha u_{0s}\frac{\partial}{\partial z} + \frac{\partial}{\partial t} - \frac{u_{0s}}{2r_+} + \frac{\mathrm{i}\alpha q_s\gamma_{0s}n_{0s}B_0}{\rho_{0s}}\right)\frac{\partial\delta v_s}{\partial t}$$
$$-\frac{\alpha q_s\gamma_{0s}n_{0s}}{\rho_{0s}}\left(\alpha u_{0s}\frac{\partial}{\partial z} + \frac{\partial}{\partial t} + \frac{u_{0s}}{2r_+}\right)\delta E = 0. \tag{49}$$

Poisson's equation (30) and (33) are linearized to obtain, respectively,

$$\frac{\partial\delta E_z}{\partial z} = 4\pi e(n_{02}\gamma_{02} - n_{01}\gamma_{01}) + 4\pi e(\gamma_{02}\delta n_2 - \gamma_{01}\delta n_1)$$
$$+ 4\pi e(n_{02}u_{02}\gamma_{02}^3\delta u_2 - n_{01}u_{01}\gamma_{01}^3\delta u_1), \tag{50}$$

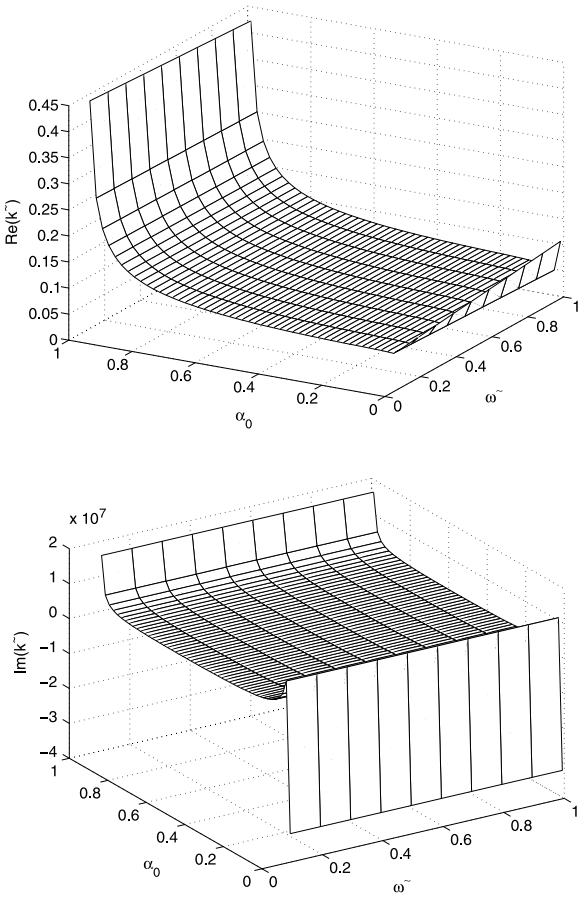

Fig. 5 *Top*: Real part of Alfvén mode for the electron-ion plasma. *Bottom*: Imaginary part of Alfvén damping and growth mode

$$\left(\alpha^2\frac{\partial^2}{\partial z^2}+\frac{3\alpha}{2r_+}\frac{\partial}{\partial z}-\frac{\partial^2}{\partial t^2}+\frac{1}{(2r_+)^2}\right)\delta E=4\pi e\alpha\left(n_{02}\gamma_{02}\frac{\partial\delta v_2}{\partial t}-n_{01}\gamma_{01}\frac{\partial\delta v_1}{\partial t}\right). \quad (51)$$

6 Local Approximation

We restrict our consideration to effects on a local scale for which the distance from the horizon does not vary significantly. We use a local (or mean-field) approximation for the lapse function and hence for the equilibrium fields and fluid quantities. If the plasma is situated relatively close to the horizon, $\alpha^2 \ll 1$, then a relatively small change in distance z will make a significant difference to the magnitude of α. Hence it is important to choose a sufficiently small range in z so that α does not vary much.

We consider thin layers in the $\mathbf{e}_{\hat{z}}$ direction, each layer with its own α_0, where α_0 is some mean value of α within a particular layer. Then a more complete picture can be built up by considering a large number of layers within a chosen range of α_0 values.

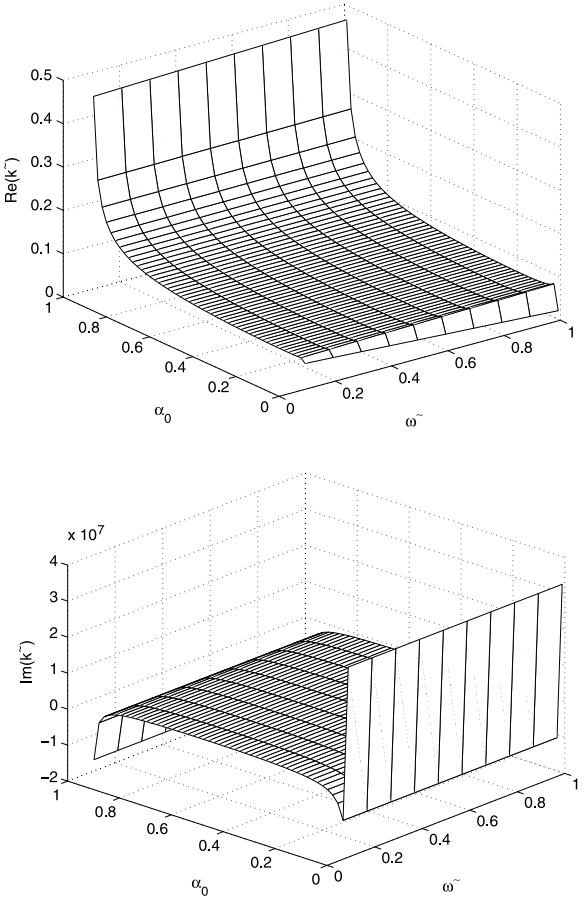

Fig. 6 *Top*: Real part of Alfvén mode for the electron-ion plasma. *Bottom*: Imaginary part of growth and damped Alfvén mode

The local approximation imposes the restriction that the wavelength must be smaller in magnitude than the scale of the gradient of the lapse function α, i.e.,

$$\lambda < \left(\frac{\partial \alpha}{\partial z}\right)^{-1} = 2r_+ \simeq \eta\, 5.896 \times 10^5 \text{ cm},$$

or, equivalently,

$$k > \frac{2\pi}{2r_+} \simeq \eta^{-1} 1.067 \times 10^{-5} \text{ cm}^{-1}, \quad 0.5 \leq \eta \leq 1,$$

for a black hole of mass $\sim 1\ M_\odot$. The value for $\eta = 0.5$ corresponds to the extremal black hole and that for $\eta = 1$ to Schwarzschild black hole.

The drawback of the hydrodynamical approach is that it is essentially a bulk, fluid approach. So the microscopic behavior of the two-fluid plasma is treated in a somewhat approximate manner via the equation of state. Then the results are really only strictly valid in the long wavelength limit. However, the restriction, imposed by the local approximation, on the wavelength is not too severe and permits the consideration of intermediate to long wavelengths so that the small k limit is still valid.

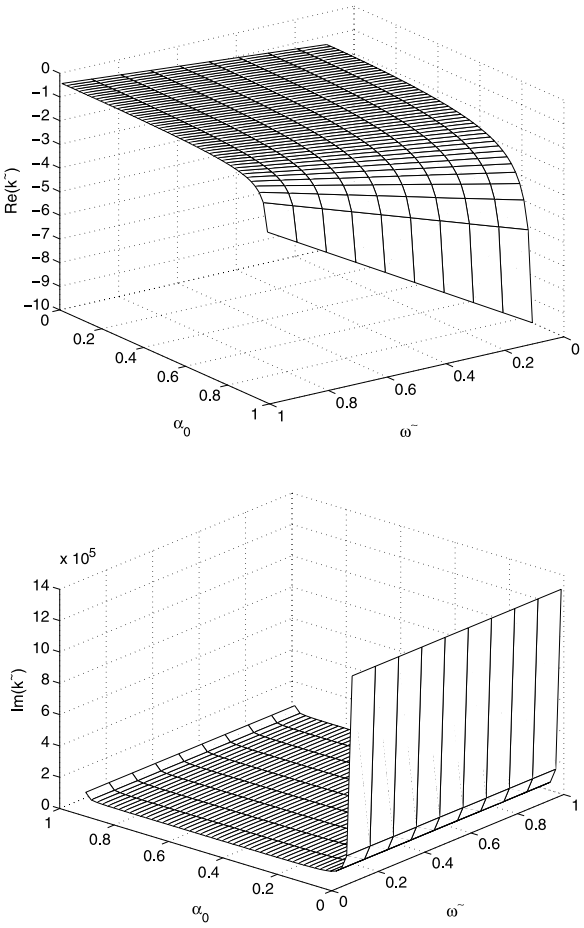

Fig. 7 *Top*: Real part of Alfvén mode for the electron-ion plasma. *Bottom*: Imaginary part of damped mode

In the local approximation for α, $\alpha \simeq \alpha_0$ is valid within a particular layer. Hence, the unperturbed fields and fluid quantities and their derivatives, which are functions of α, take on their corresponding "mean-field" values for a given α_0. Then the coefficients in (46), (49), and (50) are constants within each layer with respect to α (and therefore z as well). So it is possible to Fourier transform the equations with respect to z, using plane-wave-type solutions for the perturbations of the form $\sim e^{\mathrm{i}(kz-\omega t)}$ for each α_0 layer.

7 Dispersion Relation

When Fourier transformed, (49) and (51) become

$$\delta E = \frac{\mathrm{i}4\pi e\alpha_0\omega(n_{02}\gamma_{02}\delta v_2 - n_{01}\gamma_{01}\delta v_1)}{\alpha_0 k(\alpha_0 k - \mathrm{i}3/2r_+) - \omega^2 - 1/(2r_+)^2}, \tag{52}$$

$$\omega\left(\alpha_0 k u_{0s} - \omega + \frac{\mathrm{i}u_{0s}}{2r_+} + \frac{\alpha_0 q_s \gamma_{0s} n_{0s} B_0}{\rho_{0s}}\right)\delta v_s$$

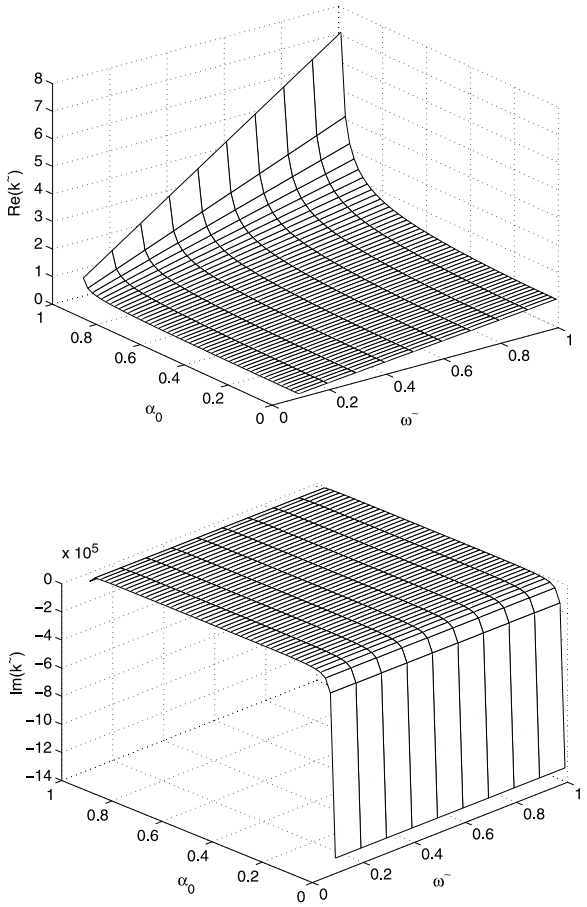

Fig. 8 *Top*: Real part of Alfvén mode for the electron-ion plasma. *Bottom*: Imaginary part of Alfvén growth mode

$$-\mathrm{i}\alpha_0 \frac{q_s \gamma_{0s} n_{0s}}{\rho_{0s}} \left(\alpha_0 k u_{0s} - \omega - \frac{\mathrm{i} u_{0s}}{2r_+} \right) \delta E = 0. \tag{53}$$

Then the dispersion relation for the transverse electromagnetic wave modes may be put in the form

$$\left[K_\pm \left(K_\pm \pm \frac{\mathrm{i}}{2r_+} \right) - \omega^2 + \frac{1}{(2r_+)^2} \right] = \alpha_0^2 \left\{ \frac{\omega_{p1}^2 (\omega - u_{01} K_\pm)}{(u_{01} K_\mp - \omega - \alpha_0 \omega_{c1})} + \frac{\omega_{p2}^2 (\omega - u_{02} K_\pm)}{(u_{02} K_\mp - \omega + \alpha_0 \omega_{c2})} \right\}, \tag{54}$$

for either the electron-positron or electron-ion plasma. Here, $\omega_{cs} = e\gamma_{0s} n_{0s} B_0 / \rho_{0s}$ and $K_\pm = \alpha_0 k \pm \mathrm{i}/2r_+$. The cyclotron frequency ω_{cs}, as well as the plasma frequency, is frame independent. Although the fluid quantities are measured in the fluid frame, the field B_0 is measured in the FIDO frame. Hence, the factors of γ_{0s} do not cancel out explicitly. The transformation $B_0 \to \gamma_{0s} B_0$ boosts the fluid frame for either fluid and thereby cancels the γ_{0s} factors. The $+$ and $-$ denote the left (L) and right (R) modes, respectively. The dispersion relation for the L mode is obtained by taking the complex conjugate of the dispersion

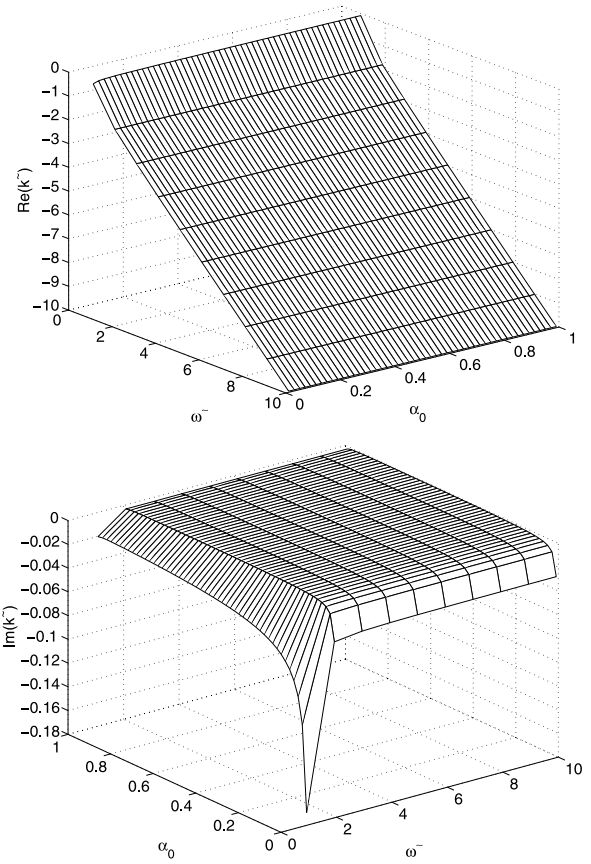

Fig. 9 *Top*: Real part of Alfvén mode for the electron-ion plasma. *Bottom*: Imaginary part of Alfvén growth mode

relation for the R mode. The two modes have the same dispersion relation in the special relativistic case.

8 Numerical Solution Modes

The dispersion relations (54) are complicated enough, even in the simplest cases for the electron-positron plasma where both species are assumed to have the same equilibrium parameters, and an analytical solution is cumbersome and unprofitable. We solve numerically the dispersion relation in order to determine all the physically meaningful modes for the transverse waves. We put the equations in the form of a matrix equation as follows:

$$(A - kI)X = 0. \tag{55}$$

The eigenvalue is chosen to be the wave number k, the eigenvector X is given by the relevant set of perturbations, and I is the identity matrix.

We need to write the perturbation equations in an appropriate form. We introduce the following set of dimensionless variables:

$$\tilde{\omega} = \frac{\omega}{\alpha_0 \omega_*}, \qquad \tilde{k} = \frac{kc}{\omega_*}, \qquad k_+ = \frac{1}{2r_+\omega_*},$$

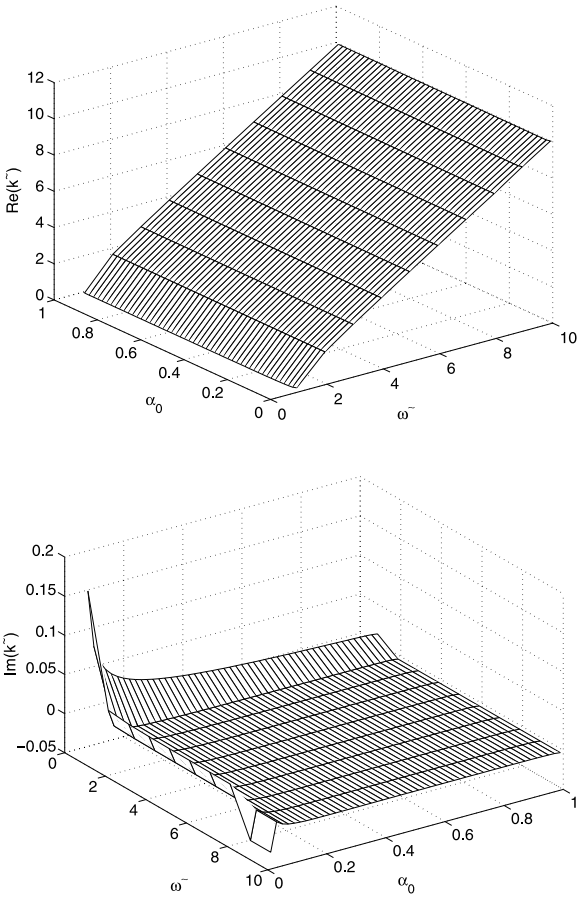

Fig. 10 *Top*: Real part of high frequency transverse mode for the electron-positron plasma. *Bottom*: Imaginary part of damping and growth mode

$$\delta\tilde{u}_s = \frac{\delta u_s}{u_{0s}}, \qquad \tilde{v}_s = \frac{\delta v_s}{u_{0s}}, \qquad \delta\tilde{n}_s = \frac{\delta n_s}{n_{0s}}, \tag{56}$$
$$\delta\tilde{B} = \frac{\delta B}{B_0}, \qquad \tilde{E} = \frac{\delta E}{B_0}, \qquad \delta\tilde{E}_z = \frac{\delta E_z}{B_0}.$$

For an electron-positron plasma, $\omega_{p1} = \omega_{p2}$ and $\omega_{c1} = \omega_{c2}$; hence, ω_* is defined as

$$\omega_* = \begin{cases} \omega_c, & \text{Alfvén modes,} \\ (2\omega_p^2 + \omega_c^2)^{1/2}, & \text{high frequency modes,} \end{cases} \tag{57}$$

where $\omega_p = \sqrt{\omega_{p1}\omega_{p2}}$ and $\omega_c = \sqrt{\omega_{c1}\omega_{c2}}$. However, for the case of an electron-ion plasma, the plasma frequency and the cyclotron frequency are different for each fluid, and so the choice of ω_* is a more complicated matter. For simplicity, we assume that

$$\omega_* = \begin{cases} \frac{1}{\sqrt{2}}(\omega_{c1}^2 + \omega_{c2}^2)^{1/2}, & \text{Alfvén modes,} \\ (\omega_{*1}^2 + \omega_{*2}^2)^{1/2}, & \text{high frequency modes,} \end{cases} \tag{58}$$

where $\omega_{*s}^2 = (2\omega_{ps}^2 + \omega_{cs}^2)$.

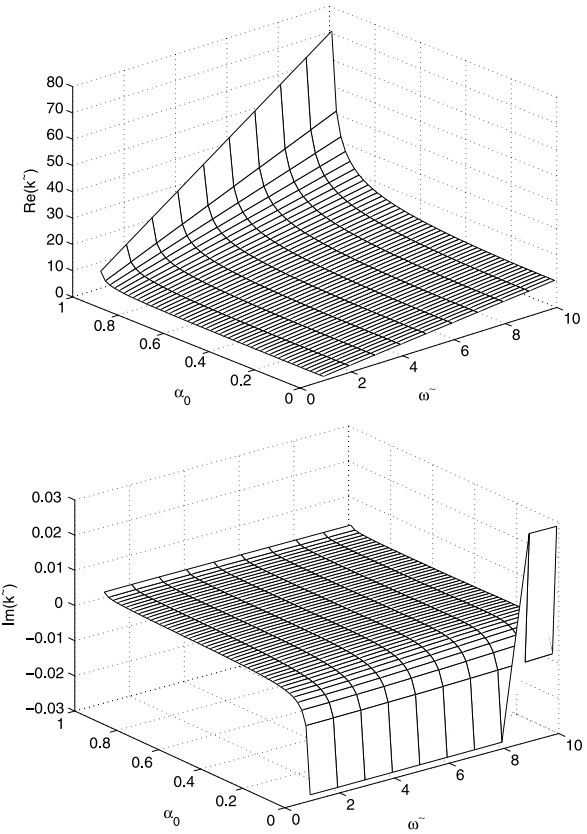

Fig. 11 *Top*: Real part of high frequency transverse mode for the electron-positron plasma. *Bottom*: Imaginary part of damping and growth mode

The dimensionless eigenvector for the transverse set of equations is

$$\tilde{X}_{\text{transverse}} = \begin{bmatrix} \delta\tilde{v}_1 \\ \delta\tilde{v}_2 \\ \delta\tilde{B} \\ \delta\tilde{E} \end{bmatrix}. \tag{59}$$

When (31) and (32) are linearized and Fourier transformed, they take the forms

$$\left(k - \frac{\mathrm{i}}{2r_+\alpha_0}\right)\delta E + \frac{\mathrm{i}\omega}{\alpha_0}\delta B = 0, \tag{60}$$

$$\frac{\mathrm{i}\omega}{\alpha_0}\delta E = \left(k - \frac{\mathrm{i}}{2r_+\alpha_0}\right)\delta B + 4\pi e(\gamma_{02}n_{02}\delta v_2 - \gamma_{01}n_{01}\delta v_1). \tag{61}$$

Using (56), we write (53), (60), and (61) in the dimensionless form:

$$\tilde{k}\delta\tilde{v}_s = \left(\frac{\tilde{\omega}}{u_{0s}} - \left(\frac{q_s}{e}\right)\frac{\omega_{cs}}{u_{0s}\omega_*} - \frac{\mathrm{i}k_+}{\alpha_0}\right)\delta\tilde{v}_s + \left(\frac{q_s}{e}\right)\frac{\omega_{cs}}{u_{0s}\omega_*}\delta\tilde{B} - \mathrm{i}\left(\frac{q_s}{e}\right)\frac{\omega_{cs}}{u_{0s}^2\omega_*}\delta\tilde{E}, \tag{62}$$

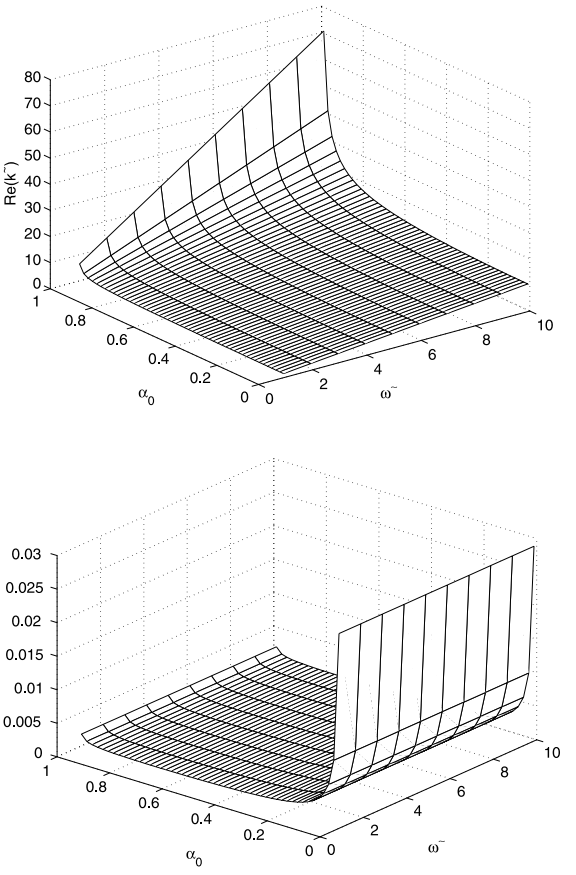

Fig. 12 *Top*: Real part of high frequency transverse mode for the electron-positron plasma. *Bottom*: Imaginary part of damped mode

$$\tilde{k}\delta\tilde{E} = -\mathrm{i}\tilde{\omega}\delta\tilde{B} + \frac{\mathrm{i}k_+}{\alpha_0}\delta\tilde{E}, \tag{63}$$

$$\tilde{k}\delta\tilde{B} = u_{01}\frac{\omega_{p1}^2}{\omega_{c1}\omega_*}\delta\tilde{v}_1 - u_{02}\frac{\omega_{p2}^2}{\omega_{c2}\omega_*}\delta\tilde{v}_2 + \frac{\mathrm{i}k_+}{\alpha_0}\delta\tilde{B} + \mathrm{i}\tilde{\omega}\delta\tilde{E}. \tag{64}$$

These are the equations in the required form to be used as input to (55).

9 Results

We carried out the numerical analysis using the well known MATLAB. We chose $\zeta^2 = 1.05$ and $q^2/M^2 = 0.2$. We have considered both the electron-positron plasma and the electron-ion plasma. The limiting horizon values for the electron-positron plasma are taken to be

$$n_{+s} = 10^{18}\ \mathrm{cm}^{-3}, \qquad T_{+s} = 10^{10}\ \mathrm{K}, \qquad B_+ = 3\times 10^6\ \mathrm{G}, \quad \text{and} \quad \gamma_g = \frac{4}{3}. \tag{65}$$

For the electron-ion plasma, the ions are essentially nonrelativistic, and the limiting horizon values are chosen to be

$$n_{+1} = 10^{18}\ \mathrm{cm}^{-3}, \quad T_{+1} = 10^{10}\ \mathrm{K}, \qquad n_{+2} = 10^{15}\ \mathrm{cm}^{-3}, \quad T_{+2} = 10^{12}\ \mathrm{K}. \tag{66}$$

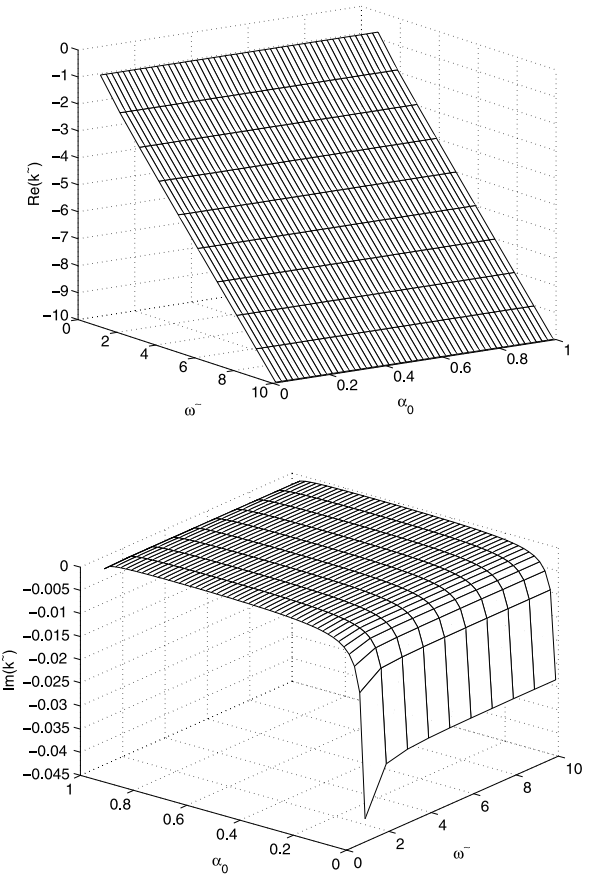

Fig. 13 *Top*: Real part of high frequency transverse mode for the electron-ion plasma. *Bottom*: Imaginary part of growth mode

The equilibrium magnetic field has the same value as it has for the electron-positron case. The gas constant and the mass and charge of the black hole have been chosen as follows:

$$\gamma_g = \frac{4}{3}, \qquad M = 5\ M_\odot, \qquad q^2 = 0.2\ M^2. \tag{67}$$

9.1 Alfvén Modes

9.1.1 Electron-Positron Plasma

For the electron-positron plasma there are four Alfvén modes as shown in Figs. 1–4. The Alfvén modes in the presence of the black hole's gravitational field are interesting in that: although the two modes, shown in Figs. 1 and 2, for electron-positron are respectively complex conjugates of the modes, shown in Figs. 3 and 4, all the modes are different for electron-ion plasma.

In the study by SK for the special relativistic case, only one purely real Alfvén mode was found to exist for the ultrarelativistic electron-positron plasma. This is because both the left and right circularly polarized modes were described by the same dispersion relation. The Schwarzschild case, investigated by BHT, admits the similar Alfvén modes as those of

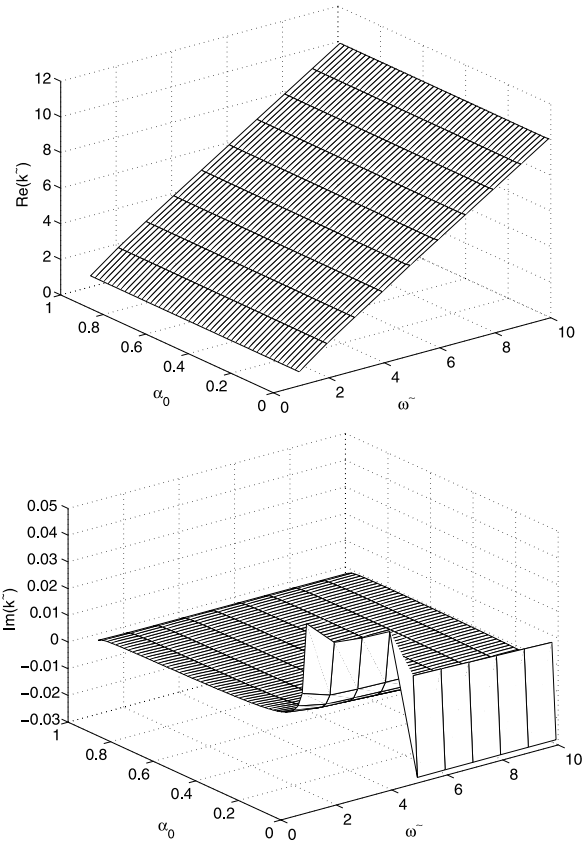

Fig. 14 *Top*: Real part of high frequency transverse mode for the electron-ion plasma. *Bottom*: Imaginary part of damping and growth mode

ours. Here $\mathrm{Im}(k) > 0$ corresponds to damping and $\mathrm{Im}(k) < 0$ to growth. This is because the convention we have used is $e^{ikz} = e^{i[\mathrm{Re}(k)+i\mathrm{Im}(k)]z}$.

9.1.2 Electron-Ion Plasma

In this case four modes are seen to exist. The first two modes, shown in Figs. 5 and 6, are a complex conjugate pair and are significantly damped and growing, respectively, whereas the other two modes, shown in Figs. 7 and 8, demonstrate only marginal damping and growth, respectively, and are equivalent to the electron-positron modes described earlier.

The differences in the magnitudes of the ω_{c1} and ω_{c2} for the first two modes apparently lead to take the frequencies from their negative (and therefore unphysical) values for the electron-positron case to positive physical values for the electron-ion case. These changes are thus because of the difference in mass and density factors as between the positrons and ions.

These four modes for electron-ion plasma are similar to those of BHT for the Schwarzschild case. It is evident that the growth and damping rates are independent of the frequency, but depended only on the distance from the black hole horizon through α_0.

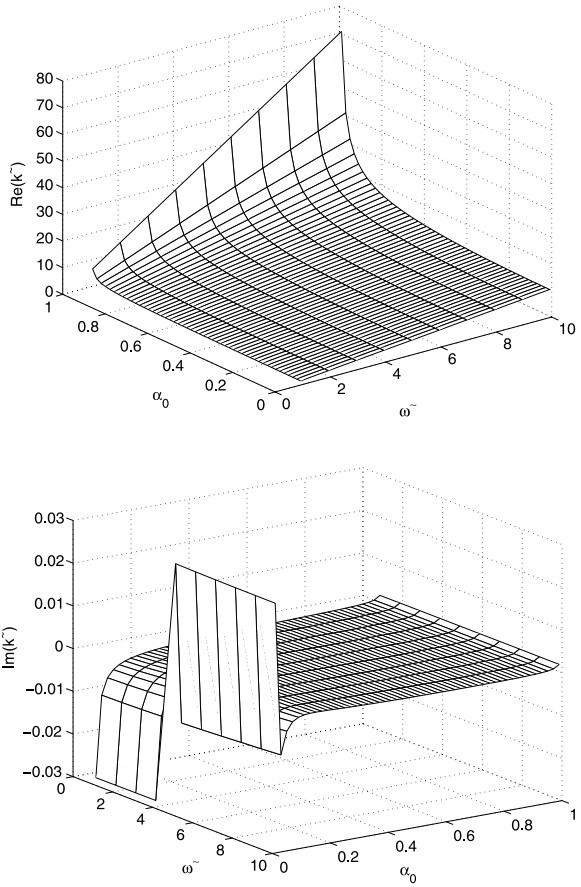

Fig. 15 *Top*: Real part of high frequency transverse mode for the electron-ion plasma. *Bottom*: Imaginary part of damping and growth mode

9.2 High Frequency Transverse Modes

9.2.1 Electron-Positron Plasma

In this case there exist four high frequency electromagnetic modes, as shown in Figs. 9–12. Figure 9 shows a small amount of growth for lower frequency $\tilde{\omega} \to 1$ and for all values of α_0.

The mode in Fig. 10 is damped for frequency $\tilde{\omega} \to 1$ but shows growth for higher frequencies $\tilde{\omega} > 6$. In special relativistic case, as was investigated by SK, there exists only one purely high frequency mode for the ultrarelativistic electron-positron plasma.

Figure 11 is similar to Fig. 12, and is growth for all frequency $\tilde{\omega} < 8$, but damped for $\tilde{\omega} > 8$. These modes are similar to those of BHT for the Schwarzschild case. The dependence of the growth and decay rates on frequency is clearly evident, unlike the corresponding Alfvén modes.

9.2.2 Electron-Ion Plasma

Like the electron-positron plasma, the electron-ion plasma admits four high frequency modes, of which two are, shown in Figs. 13 and 16, purely damped and growth, respectively.

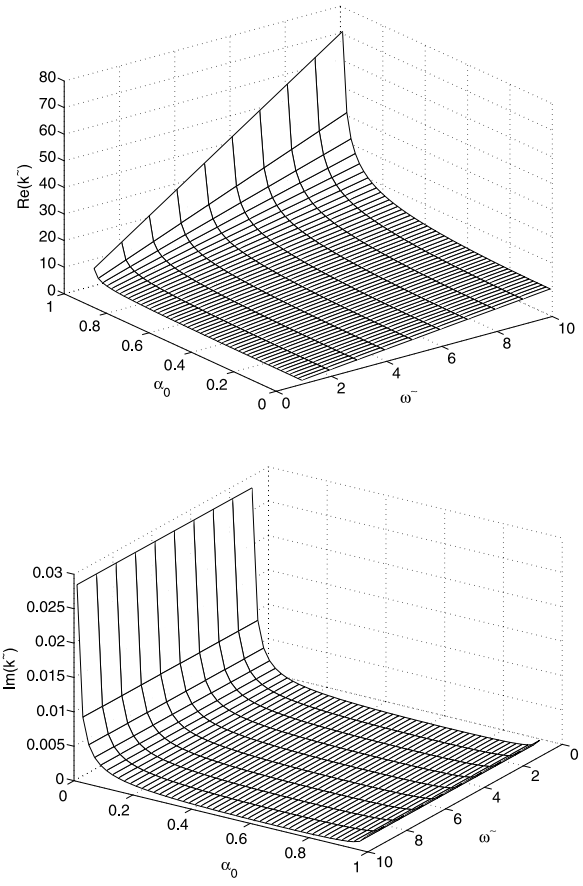

Fig. 16 *Top*: Real part of high frequency transverse mode for the electron-ion plasma. *Bottom*: Imaginary part of damped mode

The other two modes, shown in Figs. 14 and 15, are both damping and growth, respectively. Figure 14 is damped mode for all frequency $\tilde{\omega} < 5$, but shows growth for $\tilde{\omega} > 5$.

Figure 15 shows growth for all frequency $\tilde{\omega} < 3$, but damped for $\tilde{\omega} > 3$ close to the black hole event horizon. This is because the solution is too close to a resonance frequency. Unlike the first three, this mode is stable for all frequencies and at all distances from the horizon. The dependence of the growth and decay rates on frequency is clearly evident, unlike the corresponding Alfvén modes. These four modes are analogous to the three modes of BHT for the Schwarzschild case.

10 Concluding Remarks

The main concern of this study has been exclusively the investigation, within the local approximation, of Alfvén and high frequency transverse electromagnetic waves in a two-dimensional plasma surrounding the Reissner–Nordström black hole.

We derive the dispersion relations for the Alfvén and high frequency electromagnetic waves by using a local approximation and give their numerical solutions. In the limit of zero gravity our results reduce to those in special relativity obtained by Sakai and Kawata [14].

Unlike the SK work in special relativity, new modes (damped or growth) arise for the Alfvén and high frequency electromagnetic waves because of the black hole's gravitational field. For the electron-positron plasma, the damping and growth rates are smaller in general, by several orders of magnitude, compared with the real components of the wave number. But there exist modes, for the electron-ion plasma, for which the damping and growth rates are significant. This is true for the Alfvén waves in particular. For the Alfvén waves, the damping and growth rates are obviously frequency independent, but are dependent on the radial distance from the horizon as denoted by the mean value of the lapse function α_0. This is of course not the case for the high frequency waves. In that case the rate of damping or growth is dependent on both frequency and radial distance from the horizon.

Damped modes demonstrate, at least in this approximation, that energy is being drained from some of the waves by the gravitational field. The majority of the modes are growth rates and that indicate that the gravitational field is feeding energy into the waves.

The presence of magnetic monopole charge in the RN hole and the characteristic of the extremal RN hole draw attention of the physicists. In view of these reasons, our study of transverse wave propagation in relativistic two-fluid plasma in the environment close to the event horizon of the RN black hole is interesting. The result we obtained reduces to that of the Schwarzschild black hole [12] when $q = 0$. Our result can be specialized for the extreme RN hole by choosing $M^2 = q^2$. In a subsequent paper we shall study the longitudinal waves together with the two-stream instability in the environment of the RN black hole. We shall further extend our study to the Reissner–Nordström black hole spacetime generalized with cosmological parameter. This type of extension may be interesting from the point of view of an inflationary scenario of the early universe.

References

1. Thorne, K.S., Macdonald, D.A.: Mon. Not. R. Astron. Soc. **198**, 339 (1982)
2. Macdonald, D.A., Thorne, K.S.: Mon. Not. R. Astron. Soc. **198**, 345 (1982)
3. Price, R.H., Thorne, K.S.: Phys. Rev. D **33**, 915 (1986)
4. Thorne, K.S., Price, R.H., Macdonald, D.A.: Black Holes: The Membrane Paradigm. Yale University Press, New Haven (1986)
5. Zhang, X.-H.: Phys. Rev. D **39**, 2933 (1989)
6. Zhang, X.-H.: Phys. Rev. D **40**, 3858 (1989)
7. Holcomb, K.A., Tajima, T.: Phys. Rev. D **40**, 3809 (1989)
8. Holcomb, K.A.: Astrophys. J. **362**, 381 (1990)
9. Dettman, C.P., Frankel, N.E., Kowalenko, V.: Phys. Rev. D **48**, 5655 (1993)
10. Arnowitt, R., Deser, S., Misner, C.W.: In: Witten, L. (ed.) Gravitation: An Introduction to Current Research. Wiley, New York (1962)
11. Evans, C.R., Smarr, L.L., Wilson, J.R.: In: Norman, M., Winkler, K.H. (eds.) Astrophysical Radiation Hydrodynamics. Reidel, Dordrecht (1986)
12. Buzzi, V., Hines, K.C., Treumann, R.A.: Phys. Rev. D **51**, 6663 (1995)
13. Buzzi, V., Hines, K.C., Treumann, R.A.: Phys. Rev. D **51**, 6677 (1995)
14. Sakai, J., Kawata, T.: J. Phys. Soc. Jpn. **49**, 747 (1980)
15. Hajicek, P.: Nucl. Phys. B **185**, 254 (1981)
16. Gibbons, G.W.: In: Breitenlohner, P., Durr, H.P. (eds.) Proceedings of the Heisenberg Symposium. Springer, Berlin (1982)
17. Aichelberg, P.C., Güven, R.: Phys. Rev. D **24**, 2066 (1981)
18. Aichelberg, P.C., Güven, R.: Phys. Rev. D **27**, 456 (1983)
19. Aichelberg, P.C., Güven, R.: Phys. Rev. Lett. **51**, 1613 (1983)
20. Das, A., Freedman, D.Z.: Nucl. Phys. B **120**, 221 (1977)
21. Fradkin, E.S., Vasiliev, M.A.: Lebedev Institute. Preprint, No. 197 (1976)
22. Harvey, J.A., Strominger, A.: Quantum aspects of black holes. In: Harvey J., Iengo, R., Narain, K.S., Randjbar-Daemi, S., Verlinde, H. (eds.) String Theory and Quantum Gravity '92. Proceedings of the Trieste Spring School and Workshop ICTP, Trieste, Italy, March 30–April 10, 1992. World Scientific, Singapore (1993)

23. Gibbons, G., Hull, C.M.: Phys. Let. B **109**, 190 (1982)
24. Horowitz, G.T.: The dark side of string theory: black holes and black strings. In: Harvey J., Iengo, R., Narain, K.S., Randjbar-Daemi, S., Verlinde, H. (eds.) String Theory and Quantum Gravity '92. Proceedings of the Trieste Spring School and Workshop ICTP, Trieste, Italy, March 30–April 10, 1992. World Scientific, Singapore (1993)
25. Brill, D.: Phys. Rev. D **46**, 1560 (1992)
26. Colpi, M., Maraschi, L., Treves, A.: Astrophys. J. **280**, 319 (1984)
27. Harris, E.: Phys. Rev. **108**, 1357 (1957)
28. Jüttner, F.: Ann. Phys. **34**, 856 (1911) (Leipzig)